Revised Version Submitted July 2019

Fabrication of A Three-Dimensional Plasmon Ruler Using an Atomic Force Microscope

JianingLu,[a] ShaodingLiu,[c] Sean S. E. Collins,[a] LinlongTang,[b]

Xingzhan Wei,*[a,b] and Paul Mulvaney*[a]

a ARC Centre of Excellence in Exciton Science, School of Chemistry, University of Melbourne, Parkville, VIC., 3010, Australia.

b Chongqing Institute of Green and Intelligent Technology, Chinese Academy of Sciences, Chongqing, 400714, China.

c Key Lab of Advanced Transducers and Intelligent Control System of Ministry of Education, and Department of Physics and Optoelectronics, Taiyuan University of Technology, Taiyuan 030024, P. R. China

Corresponding Authors

- E-mail: weixingzhan@cigit.ac.cn
- E-mail: mulvaney@unimelb.edu.au

Abstract

We have assembled a 3D plasmon ruler using an atomic force microscope (AFM) tip to manipulate single gold nanocrystals on top of electron beam lithography (EBL) fabricated base layers. The 3D structures exhibit several polarization dependent surface plasmon scattering peaks, including symmetric and asymmetric Fano resonances. We map these resonances as a function of the degree of asymmetry of the structure. We show that the coupled surface plasmon resonances are extremely sensitive to the position of the upper particle and that the resonances can be engineered and tuned using an AFM tip to move the upper nanocrystal just a few Angstroms.

1. Introduction

Noble metal nanoparticles exhibit morphology dependent absorption and scattering spectra due to the presence of localized surface plasmon resonances (LSPR)[1,2]. Under a dark-field microscope, individual metal nanoparticles can easily be observed because they scatter light intensely at wavelengths where LSPRs occur. These depend greatly on the particle properties (dielectric function, size, and shape) as well as the dielectric constant of the host medium[1-6]. When two nanoparticles are placed in close proximity, their plasmon resonances couple and generate a scattering spectrum which depends strongly on the interparticle separation[7-11]. The coupling effect has been termed a plasmon ruler, because nanometer scale changes in separation can be monitored by the colour shifts of the dimer resonance peak[12]. The one-dimensional dimer plasmon ruler has been successfully used to monitor DNAbending[13], RNA cleavage[14] and biological activities in living cells[15].

Beyond dimers, complex plasmonic superstructures, such as one-dimensional linear arrays[16], two-dimensional trimers and tetramers[17,18] as well as laterally assembled nanorod arrays[19] have also been created, which enable different sensing geometries to be utilised. More interestingly, Liu et al., have reported a complicated 3D plasmon ruler composed of five nanorods precisely arranged in three layers[20]. The 3D structure was fabricated by combining high-precision, electron beam lithography

(EBL) and layer-by-layer, stacking techniques. Their optical measurements revealed double plasmon-induced transparency, and this was used to monitor conformational changes during complex macromolecular and biological processes. However, the shortest distance between two adjacent rods in their EBL fabricated 3D structures was 30 nm, which led to relatively weak coupling and electric field enhancement, compared to superstructures created by the DNA assembly method[21]. In order to obtain strong coupling, separations < 5nm are necessary, which is beyond the resolution of EBL. Accordingly, Barrow et al. presented a DNA assisted self-assembly method for fabricating well-defined and strongly coupled 3D nanosphere structures including tetrahedra, 3D pentamers and hexamers[21]. These structures evinced drastically enhanced local fields, 1000 times higher than the incident field strength within the 0.5 nm sized particle interstices. However, the yield of the 3D assemblies was quite low (around 1%), and furthermore the location of the upper nanoparticle and bottom structures could not be dynamically adjusted. Other methods have also been developed for creating strongly coupled 3D plasmon ruler systems[22-24] but the control and efficiency of chemical linking procedures used to create superstructures remains notoriously low. The low yield results in a small population of active plasmon rulers embedded within a large population of disordered nanoparticle aggregates, which generate spurious background signals. The controllable fabrication of such superstructures with spatial control down to < 1nm remains a major bottleneck.

To address this, we have used an AFM to construct a 3D plasmonic structure and to explore the coupled surface plasmon resonances as a function of nanoscale changes to the particle geometry. Our result marks the first step in directed assembly of 3D plasmonic structures. AFMs can be used to move a single nanoparticle with sub-nanometre precision. Although the process can be time consuming, the advantage is that both the structure manipulation and the imaging of the evolving structure can be carried out *in situ* with the AFM. Ultimately, automated AFMs could fabricate such structures routinely. However, this will require systematic understanding of the dynamics of nanocrystal friction and adhesion.

In this paper, we present a two-stage fabrication process, which combines EBL fabrication and AFM

manipulation, to build a series of 3D pentamer gold plasmonic structures. We first create a base level 2D structure of gold disks via EBL. We then move single gold nanocrystals on top of this structure with an AFM and vary the position to tune the plasmon coupling. To maintain a well-defined separation between the top sphere and the base layer, we utilise a 2nm Al_2O_3 film, fabricated via atomic layer deposition (ALD), as an ultrathin spacer layer. The immobilized nanoparticle strongly couples to the underlying nanodisks and the structure functions as a plasmon nanoruler, exhibiting distance-dependent resonance shifts in the peak scattering wavelength. Polarized dark-field microscopy (DFM) spectra are used to elucidate the plasmon modes present in each structure. The experimental spectra are then compared to finite-element method (FEM) simulations. We demonstrate that 3D plasmon rulers offer greater sensitivity than 2D dimer structures.

2. Results and Discussion

Figure 1a shows the fabrication process for the 3D clusters, which involves three main steps (EBL, ALD and AFM manipulation). Experimental details for fabrication and spectral characterization are provided in the Supporting Information. In the first step, 2D plasmonic structures are created by standard deposition and lift-off processes. In our case, we have chosen a tetramer of gold disks so that the gold particle placed on top with the AFM can maintain mechanical equilibrium. ALD is then used to deposit a 2 nm layer of Al_2O_3. The alumina layer allows a constant separation to be maintained between the particle and disks. Finally, AFM is used to pick up and deposit a single, spherical gold nanocrystal onto the structure. The deposition process is described in more detail in the Supplementary Information. Figure 1b presents AFM images before and after two sliding events; note that the upper nanosphere can be freely manipulated on top of the base disks. The position of the gold nanocrystal can be controlled to better than 0.5 nm.

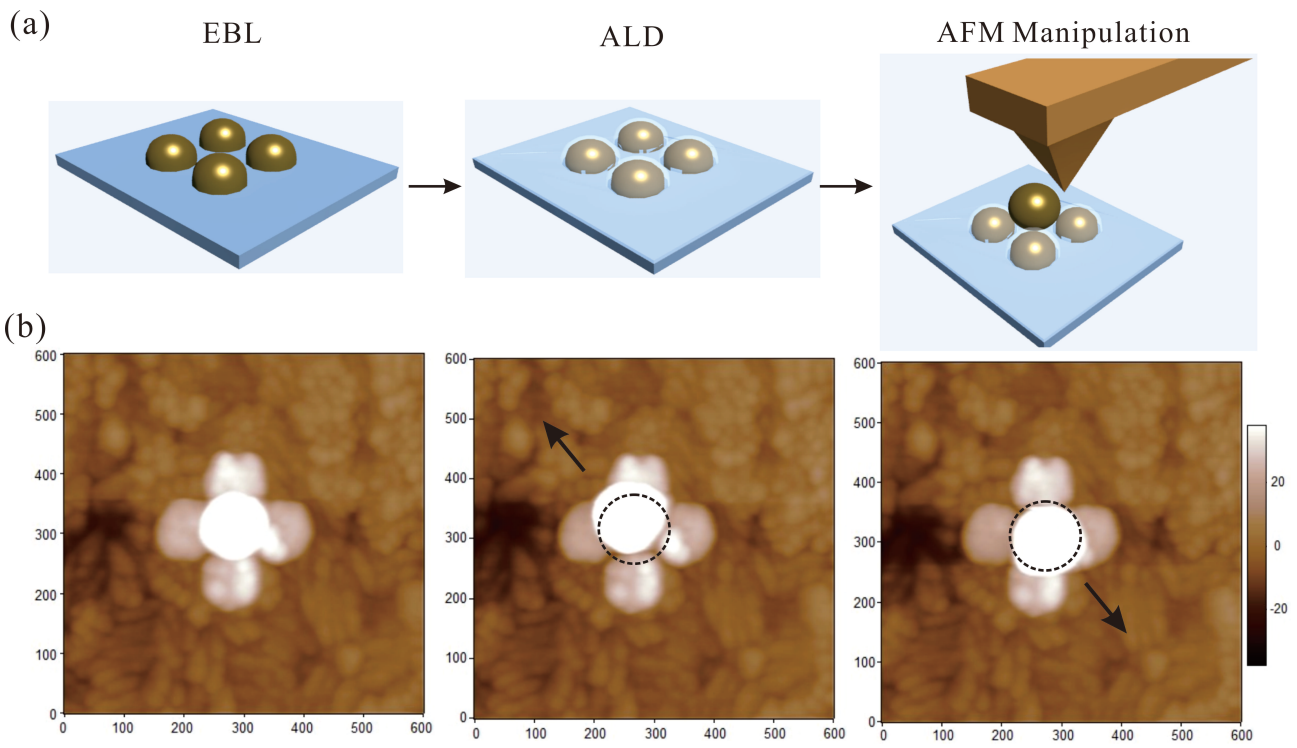

Figure 1. (a) Schematic view of the fabrication process for the 3D plasmonic clusters. The disk diameters are 80 nm, the separation is 20nm and the thickness is 35 nm. The gold nanocrystal is 85 nm in diameter but appears wider due to tip convolution[25]. (b) AFM images of the 3D pentamer before (left panel) and after translation of the top sphere (the middle and right panels). Axis labels are in nanometers. The dotted circle denotes the original location of the nanosphere before manipulation. The nanosphere was firstly moved toward the upper-left corner, indicated by the black arrow in the middle panel. The nanosphere was then moved back toward its orignial position (right panel).The image of the upper nanosphere appears to change slightly, which is an artifact due to tip convolution[25]; there is no reshaping during particle manipulation.

I. Quadrumer and Symmetric Pentamers

Figures 2a and 2b show the top and side views of the fabricated 2D quadrumer, respectively. The corresponding dark-field scattering spectra obtained with different incident light polarizations are presented in Figure 2c, where a broad resonance centered at 720 nm can be observed. The resonances are almost identical to each other because the quadrumer possesses D_{4h} point group symmetry. These experimental observations have been confirmed by FEM simulations, shown in Figure 2d, where the calculated scattering spectra, indicated by the open points, are in agreement with the measured spectra. The blue-shift of the resonances with respect to experiment are due to the refractive index and geometrical mismatches between experiment and simulation. Figure 2e

illustrates the charge distributions for the primary resonances. The dipole plasmons of individual disks oscillate in-phase, which results in a bright and superradiant collective resonance as reported in previous studies[26-28].

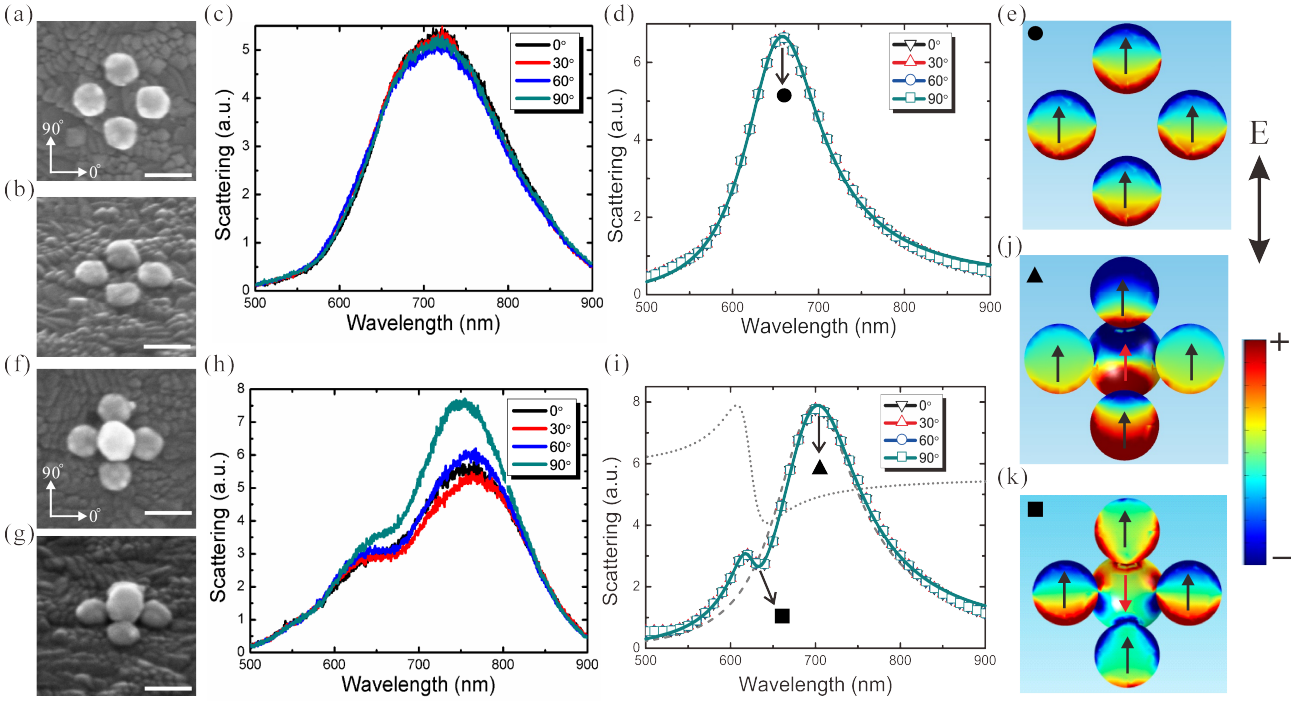

Figure 2. Characterization of the 2D symmetric quadrumer and 3D symmetric pentamer. (a) SEM top view images of the quadrumer; (b) oblique view with 50º viewing angle. The scale bar is 100 nm. (c) Measured dark-field scattering spectra of the quadrumer for different incident polarization angles. (d) Corresponding FEM simulated spectra (open points), and the fitted spectra with a symmetric pseudo-Lorentzian line shape (solid lines, Equation 2). (e) Calculated surface charge distributions at the resonance wavelength; (f) SEM top view images of the 3D symmetric pentamer; (g) oblique view with 50º viewing angle. (h) Measured dark-field scattering spectra of the pentamer for different polarization angles. (i) The FEM calculated spectra (open points), and the fitted spectra analysed using the Fano interference model (solid lines, Equation 3), where the dashed and dotted lines are the symmetric and asymmetric line shapes extracted from the fitting, respectively; (j) and (k)the charge distributions associated with the superradiant and subradiant resonances, respectively.

The optical responses change dramatically when an additional gold nanoparticle is placed on the quadrumer to form a 3D pentamer. SEM images of a fabricated 3D pentamer are presented in Figures 2f and g, where the upper nanosphere is symmetrically located atop the quadrumer. The dark-field scattering spectra shown in Figure 2h reveal that instead of a symmetric resonance, asymmetric resonances with a scattering dip around 675 nm appear in the spectra, which can be assigned to the excitation of a Fano resonance. Since the upper nanosphere is placed

symmetrically on the quadrumer, and the 3D pentamer possesses a high structural symmetry, one may expect that the optical scattering spectra will not exhibit a significant dependence on the incident polarization. However, there are minor spectral shifts for the measured scattering spectra, as seen in Figure 2h. These may be attributed to the fact that the fabricated nanodisks and nanosphere are not perfectly circular or spherical, and there may be slight distance variations between the nanosphere and the individual nanodisks, which will break the symmetry. Another symmetric pentamer with a similar morphology is shown in Figure S3 of the Supporting Information, which exhibits similar spectral trends to those in Figure 2(h); the small difference near the scattering peak is mainly due to the variation in size of the upper nanoparticle in these two cases.

Since the plasmon coupling between these two layers is quite strong at such a small separation (about 2 nm), a slight change in the separation will lead to large variations in the optical response, as shown in Figure S4 of the Supporting Information. The resonance peak wavelength red-shifts from 703 to 770 nm as the gap changes from 1 to 2 nm, and the spectral shift is around 6.7 nm for every 1 Å change in the particle-disk separation, which makes this 3D structure more sensitive than reported plasmon rulers[29]. Note that these 3D superstructures should exhibit an even more pronounced red-shift, if the gap further decreases. However, at a critical distance the gap should reach the quantum tunneling regime[30-33]. The sensitivity of the 3D plasmon ruler diminishes drastically at larger separation distances due to the nonlinearity of plasmon coupling and it is not useful once the separations exceed the particle diameter.

For the 3D symmetric pentamer, the calculated scattering spectra for different incident polarizations are identical to each other (see open points, Figure 2i). Figure 2k presents the charge distributions at 705 nm for the pentamer, where the localized surface plasmons of individual particles oscillate in-phase, resulting in a strong dipole moment and the formation of a bright, superradiant resonance. On the contrary, the surface plasmons of the sphere oscillate out-of-phase to the electron oscillations of the lower quadrumer when the excitation wavelength corresponds to the scattering dip (Figure 2j), which results in the partial cancellation of the dipole moments

and the formation of a subradiant resonance. The superradiant and subradiant resonances are spectrally overlapping and this destructive interference results in the formation of the asymmetric Fano resonance.

In order to gain deeper physical insights, a model proposed by Gallinet et al. was used to fit the calculated spectra[34], which provides a general and consistent way to characterize Fano-like resonances. The lineshape of the asymmetric resonance (AR) can be described by

$$\sigma_{AR}(\omega) = \frac{\left(\frac{\omega^2-\omega_a^2}{2W_a\omega_a}+q\right)^2+b}{\left(\frac{\omega^2-\omega_a^2}{2W_a\omega_a}\right)^2+1} \quad (1)$$

The Fano lineshape is a result of the interference between the direct excitation of the continuum and the excitation of the dark mode with coupling to the continuum. Here ω_a denotes the resonance frequency, W_a is the spectral width, q is the asymmetry parameter, and b denotes the modulation damping parameter, which, in turn, depends on the ratio between the intensity lost to the metallic structure and the intensity transferred from the bright mode to the dark mode. The bright mode, on the other hand, possesses a symmetric pseudo-Lorentzian line shape,

$$\sigma_{SR}(\omega) = \frac{a^2}{\left(\frac{\omega^2-\omega_s^2}{2W_s\omega_s}\right)^2+1} \quad (2)$$

where a is the amplitude, and ω_s and W_s are the resonance frequency and the linewidth, respectively. Then the scattering spectrum of the structure can be written as the product of the bright (SR) and dark (AR) modes,

$$\sigma(\omega) = \sigma_{SR}(\omega)\sigma_{AR}(\omega) \quad (3)$$

Since only a bright mode is excited in the case of the 2D quadrumer, the simulated spectra can be well-fitted to Equation 2 (solid lines, Figure 2d). On the other hand, a Fano resonance is excited for the 3D pentamer, and the fitted spectra using Equation 3 agree with that of the numerical simulations (solid lines, Figure 2i), and the dashed and dotted lines denote the normalized symmetric and asymmetric resonances, respectively. The extracted fitting parameters are reported

in Table 1. Compared to that of the quadrumer, the amplitude (a) of the SR is enlarged due to the coupling between the gold structures in the two layers, and the resonance (ω_s) red-shifts from 1.885 eV to about 1.772 eV. The linewidth of the AR (W_a) is only about 0.056 eV, and it is much narrower than that of the symmetric resonance (W_s = 0.152 eV). In addition, energy detuning occurs between the SR and AR, the asymmetry parameter is relatively large (q = 0.328), and the modulation damping parameter b = 0.947, indicating a strong damping of the structure.

TABLE 1. Fitting parameters for the planar quadrumer and 3D pentamers using the Fano interference model.

	Polarization	*a*	ω_s (eV)	W_s(eV)	ω_a(eV)	W_a(eV)	*q*	*b*
Figure 2d		0.258	1.886	0.159				
Figure 2i		0.307	1.772	0.152	1.991	0.056	0.328	0.947
Figure 3d	0°	0.313	1.764	0.149	1.993	0.057	0.398	0.916
	90°	0.264	1.816	0.173				
Figure 5c	0°	0.455	1.634	0.124	1.937	0.098	0.903	0.961
	90°	0.285	1.805	0.173				

II. Weakly Asymmetric Pentamers

The optical responses of plasmonic oligomer clusters are governed by the structural symmetry and the collective plasmon resonances are expected to be strongly modified when the structural symmetry is broken. For example, the symmetry of the 3D pentamer will be lowered to C_{2v} point group when the upper nanosphere shifts slightly away from the center point of the quadrumer, and polarization dependent responses would be observed in this situation. The practical outcome of the distance-dependent variations in the optical response is that the pentamer can be used for sensing the position of the nanosphere or as a 3D plasmon ruler. Figures 3a and 3b show SEM images of the modified pentamer, where the upper nanosphere is moved about 5 nm away from the center point. The measured dark-field scattering spectra shown in Figure 3c reveal that an asymmetric Fano resonance appears in the spectrum when the polarization angle $\theta = 0°$. However, the modulation depth decreases with increasing polarization angle and the Fano resonance

disappears completely from the spectrum when θ = 90°; a single, almost symmetric resonance is observed in this case. These results for the asymmetric 3D pentamer are consistent with the Fano switch structure composed of asymmetric clusters[35], where the subradiant resonance cannot be excited when θ = 90°, due to the reduced coupling strength between the individual particles. Only the bright resonance can be observed in this case, and the optical responses are modified by the incident polarization.

The open points in Figure 3d show the simulated spectra of the 3D asymmetric pentamer, which agree well with the experimental results. The Fano interference model can also be used to fit the spectra, and to quantify the interactions between the SR and AR. The black line in Figure 3d represents the fitted spectrum when θ = 0°, and it agrees quantitatively with the numerical results. The fitting parameters shown in Table 1 indicate that the optical responses are similar to those of the symmetric pentamer. However, when the polarization angle θ = 90°, only the bright mode is excited, and it can be well fitted to the SR equation alone (the dark cyan line, Figure 3d). Since the symmetry of the modified pentamer belongs to the C_{2v} point group, the optical responses to any angle of incidence are given by a combination of two optical responses with orthogonal incident polarizations, weighted by the excitation intensities. Therefore, the scattering spectrum with a polarization angle θ can be written as,

$$\sigma_\theta(\omega) = \sigma_{0^\circ}(\omega)\cos^2\theta + \sigma_{90^\circ}(\omega)\sin^2\theta \quad (4)$$

The red and blue lines in Figure 3d represent the calculated spectra based on the fitting results of θ = 0° and θ = 90°, and they are in good accordance with those of the numerical simulations.

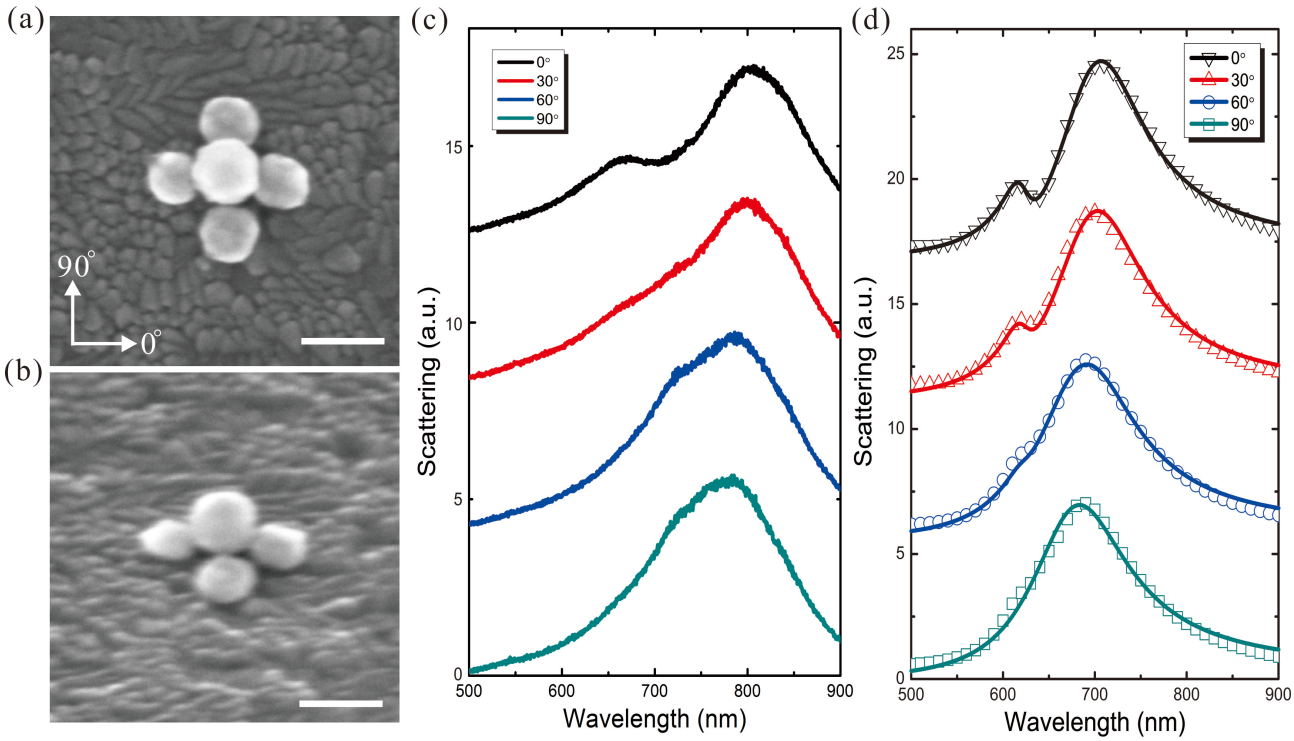

Figure3.Characterization of a 3D asymmetric pentamer with a minor shift of the upper nanosphere. (a) SEM images of the top view, and (b) the side view of the fabricated 3D asymmetric pentamer, where the upper gold nanosphere is moved about 5 nm away from the center of the quadrumer. Scale bar is 100nm. (c) Measured dark-field scattering spectra versus the incident polarization angle. (d) Corresponding FEM simulated spectra (the open points), and the fitted spectral with the analysis Fano interference model (the solid lines, Equation 3), where only the SR is considered when $\theta = 90°$, and the fitted spectra for $\theta = 30°$ and 60° are calculated based on the fitting results at $\theta = 0°$ and $\theta = 90°$ (Equation 4).

III. Strongly Asymmetric Pentamers

The optical responses can be manipulated by further adjusting the position of the nanosphere. For example, when the nanosphere is moved about 25 nm away from the center of the quadrumer along the 145º direction (Figure 4a and b), the distances to the bottom and right hand nanodisks are enlarged, thereby leading to weaker plasmon coupling. Consequently, the collective resonances are modified compared to those of the pentamer with minor symmetry breaking (Figure 3). Figure 4c presents the measured, polarization-dependent, dark-field scattering spectra. The Fano resonance is no longer excited when there is such large symmetry breaking, and only broad and symmetric resonances are observed in this situation. In addition, the modified pentamer also possesses C_{2v} point group symmetry, and the symmetry axis is along the $\theta = 145°$ direction. Therefore, the optical responses for the polarization $\theta = 0°$ and $\theta = 90°$ (as well as for $\theta = 30°$ and

θ = 60°) would be identical to each other from the symmetry point of view. The experimental results reveal that the plasmon resonance peak wavelength is about 736 nm when θ = 0° and θ = 90°, and it red-shifts to about 748 nm when θ = 30° and θ = 60°. The red-shift of the resonance can be understood by investigating the geometry of the asymmetric pentamer. When the incident electric field is aligned between the upper-left three nanoparticles i.e. when θ = 30° and θ = 60°, stronger plasmon coupling occurs, resulting in the red-shift of the collective resonance compared to excitation at polarization angles θ = 0° and θ = 90°. The FEM simulations shown in Figure 4d confirm the above experimental observations.

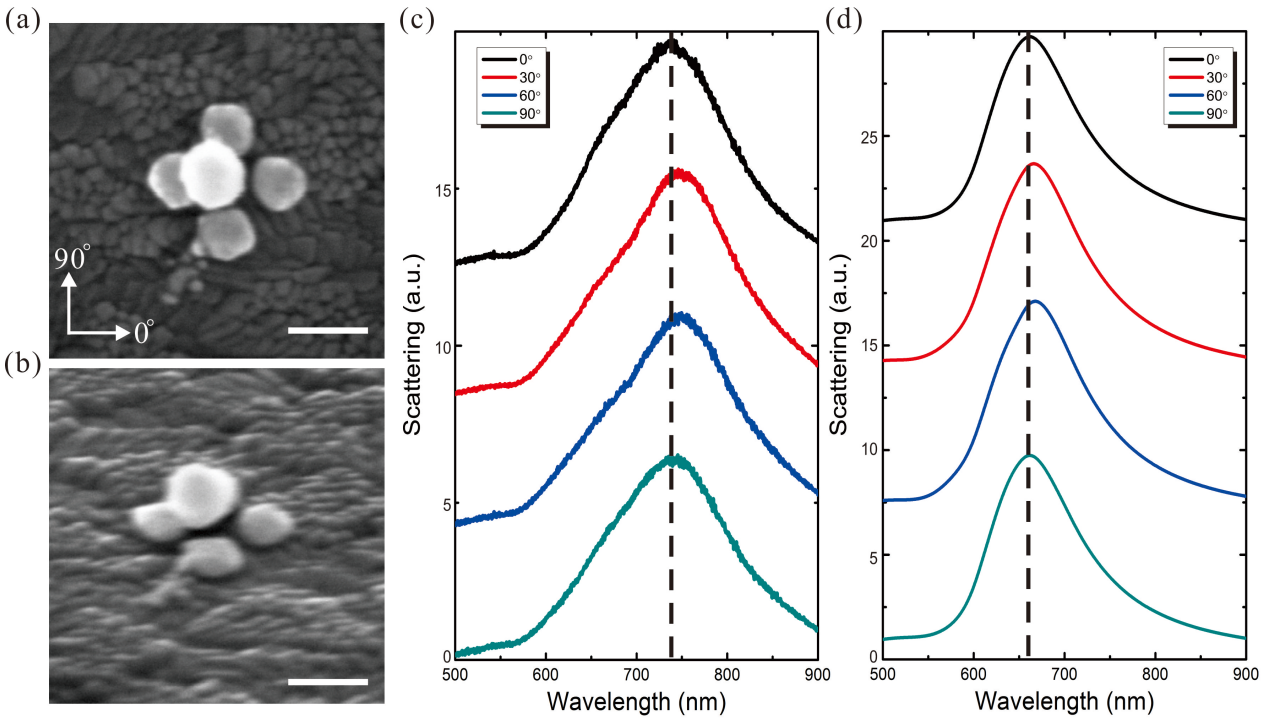

Figure 4.Characterization of a 3D asymmetric pentamer with a large shift of the upper nanosphere. (a) SEM images of the 3D asymmetric pentamer (top view); (b) side view, where the upper nanosphere is moved about 25 nm away from the center of the quadrumer along the 145º direction. Scale bar is 100nm. (c) Measured dark-field scattering spectra versus the incident polarization angle. (d) Corresponding FEM simulated spectra.

When the upper nanosphere is further shifted and moved onto one of the disks (Figures S5a and b), the separation between the nanosphere and the other three disks is much larger than in the case of the former 3D pentamers. The measured dark-field scattering spectra shown in Figure S5c indicate that the optical responses of the pentamers to the incident light polarization angle are

almost identical. The result of polarization insensitivity is similar to the case of the plasmon rulers composed of a nanoparticle dimer[12,36,37], where the variation in the plasmon resonances is very small when the distance between the two nanoparticles is relatively large. In general, the above studies demonstrate that the optical responses of the 3D pentamer can be strongly modified by adjusting the position of the nanosphere. In other words, the position of the upper nanosphere can be deduced from the polarization dependent scattering spectra. For practical applications, it is important to understand how the plasmon ruler works. The data in Figure 3 demonstrate that when the upper nanosphere shifts slightly away from the center point of the quadrumer, the optical response changes dramatically compared to the response of the symmetric cluster (Figure 2). The data also reveal that the optical response can be further modified when the nanosphere is moved about 25 nm away from the center of the quadrumer along the 145º direction (Figure 4). Therefore, the shift length from the center point, the shift angle, and separation of the lower quadrumer from the upper nanosphere can all collectively function as the variables for a 3D plasmon ruler. The scattering response will be modified when any of these parameters is modified. In turn, spectral shifts to the structure can be used to calculate the relative position and orientation of the upper nanosphere.

IV. The Rod Pentamer

The plasmon resonance should also be sensitive to the morphology of the overlying nanocrystal. In Figure 5a, a single gold nanorod with a short aspect ratio is symmetrically placed on the lower quadrumer using the AFM. The rod has a length of 100 nm, the width is about 80 nm, and the long axis of the rod is oriented along one of the symmetry axes of the quadrumer. The measured dark-field scattering spectra with different incident polarizations are shown in Figure 5b. When the polarization angle $\theta = 0°$, that is, the electric field vector lies along the major axis of the rod, an obvious Fano resonance is observed around 735 nm (the black line, Figure 5b), and the two scattering peaks are more pronounced compared to those of the pentamer composed of a

nanosphere and four nanodisks (Figure 2h). The modulation depth of the Fano resonance decreases as the polarization angle increases (the red and blue lines, Figure 5b). When the polarization is along the minor axis of the rod (θ = 90°), the Fano resonance cannot be excited, and a broad superradiant resonance appears in the spectrum (the dark cyan line, Figure 5b). The open points in Figure 5c show the corresponding FEM simulation results, which are in accordance with those of the measured spectra, and the small differences in the line widths and the spectral shifts can be attributed to minor structural differences between the experiments and the simulations.

For excitation of the Fano resonance, the simulated spectrum when θ = 0° can be well fitted by the Fano interference model (the black line, Figure 5c). The fitting parameters shown in Table 1 indicate that the scattering amplitude of the SR, a, is enhanced due to the formation of the stronger dipole moment in the rod and the resonance exhibits a red-shift to about 1.63 eV. The line width (W_a) for the AR is broader than that of the other pentamers. The asymmetry parameter q is enlarged to 0.903, so that the response has the appearance of two distinct peaks (the black line, Figure 5c). The relevant surface charge distributions associated with the subradiant and the superradiant resonances are shown in Figure 5(d) and (e), respectively. When θ = 90°, there is, in addition to the superradiant resonance around 695 nm (Figure 5f), a small kink around 650 nm in the simulated spectrum (the dark cyan line, Figure 5c); this spectral feature is very weak and can be neglected. Therefore, the scattering spectrum can be fitted to the SR model (Equation 2), and the fitted spectrum agrees well with the simulation (the dark cyan line, Figure 5c). Since the symmetry of the pentamer belongs to the D_{2h} point group, the polarization dependent scattering can also be fitted to Equation 4. The red and blue lines in Figure 5c represent, respectively, the calculated spectra when θ = 30° and θ = 60°, which agree very well with the simulations. These results further demonstrate that the optical responses of the 3D pentamer can be manipulated by adjusting the shape of the single “floating” nanocrystal, and the 3D pentamer also can be used for nanoparticle shape sensing.

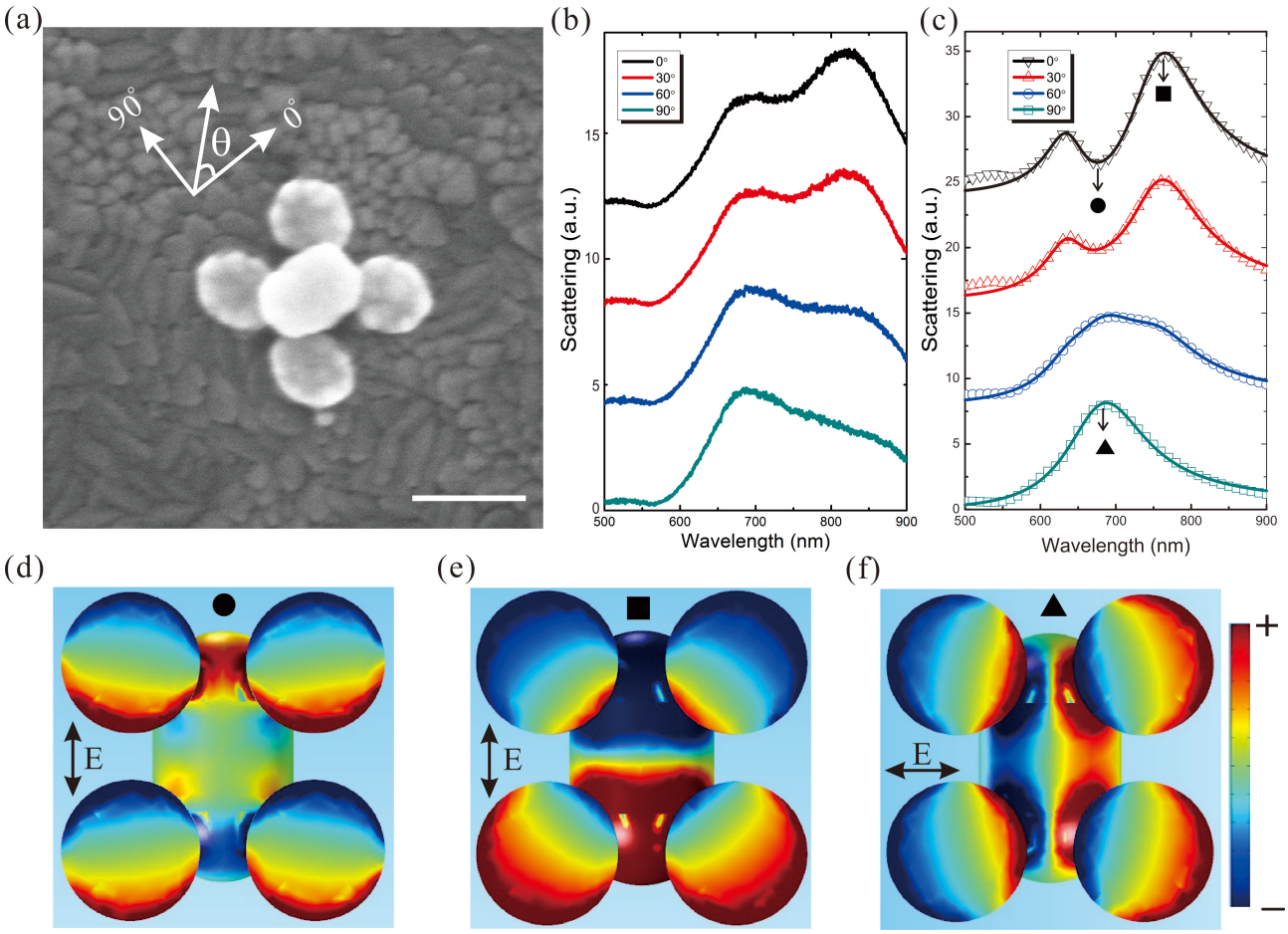

Figure 5. Optical responses of a 3D pentamer composed of a nanorod and four nanodisks. Scale bar is 100nm. (a) Top view of the fabricated 3D pentamer, where the nanorod is placed symmetrically on the quadrumer, and the long axis of the rod is along one of the symmetry axis of the quadrumer. (b) Measured dark-field scattering spectra with different incident polarizations. (c) Corresponding FEM simulations (the open points), and the fitted spectral with the analysis Fano interference model (the solid lines, Equation 3), where only the SR is considered when θ = 90°, and the fitted spectra for θ = 30° and 60° are calculated based on the fitting results of θ= 0° and 90° (Equation 4).(d) and (e) Surface charge distributions associated with the subradiant and the superradiant resonances, respectively, when θ = 0°. (f) Surface charge distributions at the peak wavelength when θ = 90°.

The use of 3D pentamers as optical reporters has several attractive features that contribute to the unique properties of plasmon rulers. Firstly, the scattering from the 3D pentamer is much brighter than that of the reported dimer[7] and the coupled film nanoparticle[29], and can be easily identified by the naked eye using DFM, which may enable their use in sensing devices at the single-molecule level. Secondly, the nanoscale gaps created between the upper nanocrystal and the base nanodisks represent tightly confined 'hot spots' where electromagnetic fields are enhanced by many orders of magnitude, which is much better than the first 3D plasmon ruler fabricated by the EBL method[20,38]. These hot spots can be used to stimulate surface enhanced resonant Raman scattering

from molecules located within the gap regions. A third advantage is that the 3D pentamer can be dynamically adjusted with nanoscale precision using the AFM, which offers better spatial resolution than the DNA self-assembly method[21-22]. Finally, the relevant optical properties of these types of plasmonic structure are completely tunable by varying the size, shape, position and composition of the upper nanoparticle, which provides more freedom for the design and application of these 3D plasmon rulers.

3. Conclusions

In summary, we have made 3D pentamer plasmon rulers for the first time by combining EBL, ALD and AFM manipulation, and have monitored the coupling of the surface plasmon modes using dark-field spectroscopy. The light scattering properties of fabricated superstructures with different position or shape of the upper nanosphere have been investigated and compared to modelling results obtained using FEM. The symmetric and asymmetric Fano resonances can be excited using different light polarizations, and the excitation peak greatly depends on the position and shape of the upper nanoparticle. The spectral shift can be as much as 6.7 nm for every 1 Å change of the particle-disk separation.

Supporting Information

The supporting information contains further experimental details including: fabrication of the nanodisk arrays, atomic layer deposition conditions, gold nanoparticle synthesis, AFM manipulation of single nanocrystals, DFM spectroscopy and modelling.

Acknowledgements

The authors thank the ARC for support through grants LF11000117, DP160102754 and CE170100026. Xingzhan Wei acknowledges the support of the National Science Foundation of China (NSFC11574308). Shaoding Liu acknowledges the support of NSFC (11874276 and 11574228), the Natural Science Foundation of Shanxi Province (201601D021005), and the San Jin Scholars Program of Shanxi Province.

References

(1)Sardar, R.; Funston, A. M.; Mulvaney, P.; Murray, R. W. Gold nanoparticles: past, present, and future. *Langmuir* **2009,***25 (24)*, 13840-13851.
(2)Grzelczak, M.; Perez-Juste, J.; Mulvaney, P.; Liz-Marzan, L. M. Shape control in gold nanoparticle synthesis. *Chem. Soc. Rev.***2008,***37 (9)*, 1783-1791.
(3)Halas, N. J.; Lal, S.; Chang, W.-S.; Link, S.; Nordlander, P. Plasmons in Strongly Coupled Metallic Nanostructures. Chem. Rev. 2011, 111 (6), 3913–3961.
(4)Wei, X.; Altissimo, M.; Davis, T. J.; Mulvaney, P. Fano Resonances in Three-Dimensional Dual Cut-Wire Pairs. Nanoscale 2014, 6 (10), 5372–5377.
(5)Wei, X.; Du, C.; Dong, X.; Luo, X.; Deng, Q.; Zhang, Y. Nanofabrication with Controllable Localization Energy Based on the Interference Modulation of Surface Plasmons. Opt. Express 2008, 16 (19), 14404.
(6)Stender, A. S.; Wei, X.; Augspurger, A. E.; Fang, N. Plasmonic Behavior of Single Gold Dumbbells and Simple Dumbbell Geometries. J. Phys. Chem. C 2013, 117 (31), 16195–16202.
(7)Nordlander, P.; Oubre, C.; Prodan, E.; Li, K.; Stockman, M. I. Plasmon hybridization in nanoparticle dimers. *Nano Lett.***2004,***4 (5)*, 899-903.
(8)Ghosh, S. K.; Pal, T. Interparticle Coupling Effect on the Surface Plasmon Resonance of Gold Nanoparticles: From Theory to Applications. Chem. Rev. 2007, 107 (11), 4797–4862.
(9)Atay, T.; Song, J.-H.; Nurmikko, A. V. Strongly Interacting Plasmon Nanoparticle Pairs: From Dipole−Dipole Interaction to Conductively Coupled Regime. Nano Lett. 2004, 4 (9), 1627–1631.
(10)Jain, P. K.; El-Sayed, M. A. Plasmonic Coupling in Noble Metal Nanostructures. Chemical Physics Letters 2010, 487 (4–6), 153–164.
(11)Brown, L. V.; Sobhani, H.; Lassiter, J. B.; Nordlander, P.; Halas, N. J. Heterodimers: Plasmonic Properties of Mismatched Nanoparticle Pairs. ACS Nano 2010, 4 (2), 819–832.
(12)Jain, P. K.; Huang, W.; El-Sayed, M. A. On the universal scaling behavior of the distance decay of plasmon coupling in metal nanoparticle pairs: a plasmon ruler equation. *Nano Lett.***2007,***7 (7)*, 2080-2088.
(13)Reinhard, B. M.; Sheikholeslami, S.; Mastroianni, A.; Alivisatos, A. P.; Liphardt, J. *Proc. Natl. Acad. Sci. U. S. A.***2007,***104 (8)*, 2667-2672.
(14)Skewis, L. R.; Reinhard, B. M. Spermidine modulated ribonuclease activity probed by RNA plasmon rulers. *Nano Lett.***2008,***8 (1)*, 214-220.
(15)Jun, Y.-W.; Sheikholeslami, S.; Hostetter, D. R.; Tajon, C.; Craik, C. S.; Alivisatos, A. P. Continuous imaging of plasmon rulers in live cells reveals early-stage caspase-3 activation at the single-molecule level. *Proc. Natl. Acad. Sci. U. S. A.***2009,***106 (42)*, 17735-17740.
(16)Barrow, S. J.; Funston, A. M.; Gomez, D. E.; Davis, T. J.; Mulvaney, P. Surface plasmon resonances in strongly coupled gold nanosphere chains from monomer to hexamer. *Nano Lett.***2011,***11 (10)*, 4180-4187.
(17)Barrow, S. J.; Funston, A. M.; Wei, X.; Mulvaney, P. DNA-directed self-assembly and optical properties of discrete 1D, 2D and 3D plasmonic structures. *Nano Today* **2013,***8 (2)*, 138-167.
(18)Kumar, J.; Wei, X.; Barrow, S.; Funston, A. M.; Thomas, K. G.; Mulvaney, P. Surface plasmon coupling in end-to-end linked gold nanorod dimers and trimers. *Phys. Chem. Chem. Phys.***2013,***15 (12)*, 4258-4264.
(19)Kumar, J.; Wei, X.; Barrow, S. J.; Funston, A. M.; Thomas, K. G.; Mulvaney, P. *Z. Phys. Chem. (Muenchen, Ger.)***2018,***232 (9-11)*, 1607-1617.
(20)Liu, N.; Hentschel, M.; Weiss, T.; Alivisatos, A. P.; Giessen, H. Three-dimensional plasmon rulers. *Science* **2011,***332 (6036)*, 1407-1410.
(21)Barrow, S. J.; Wei, X.; Baldauf, J. S.; Funston, A. M.; Mulvaney, P. The surface plasmon modes of self-assembled gold nanocrystals. *Nat. Commun.***2012,***3*, 1275
(22) Urban, A. S.; Shen, X.; Wang, Y.; Large, N.; Wang, H.; Knight, M. W.; Nordlander, P.; Chen, H.; Halas, N. J. Three-dimensional plasmonic nanoclusters. *Nano Lett.***2013,***13 (9)*, 4399-4403.
(23) Liu, H.; Yang, Z.; Meng, L.; Sun, Y.; Wang, J.; Yang, L.; Liu, J.; Tian, Z. Three-dimensional and time-ordered surface-enhanced Raman scattering hotspot matrix. *J. Am. Chem. Soc.***2014,***136 (14)*, 5332-5341.
(24) Boles, M. A.; Engel, M.; Talapin, D. V. Self-assembly of colloidal nanocrystals: From intricate structures to functional materials. *Chem. Rev.***2016,***116 (18)*, 11220-11289.
(25) Mulvaney, P.; Giersig, M. Imaging nanosized gold colloids by atomic force microscopy: a direct comparison with transmission electron microscopy. *J. Chem. Soc., Faraday Trans.***1996,***92 (17)*, 3137-3143.
(26) Rahmani, M.; Lei, D. Y.; Giannini, V.; Lukiyanchuk, B.; Ranjbar, M.; Liew, T. Y. F.; Hong, M.; Maier, S. Subgroup decomposition of plasmonic resonances in hybrid oligomers: modeling the resonance lineshape. A. *Nano Lett.***2012,***12 (4)*, 2101-2106.

(27) Hentschel, M.; Saliba, M.; Vogelgesang, R.; Giessen, H.; Alivisatos, A. P.; Liu, N. Transition from isolated to collective modes in plasmonic oligomers. *Nano Lett.***2010,***10 (7)*, 2721-2726.
(28) Fan, J. A.; Wu, C.; Bao, K.; Bao, J.; Bardhan, R.; Halas, N. J.; Manoharan, V. N.; Nordlander, P.; Shvets, G.; Capasso, F. Self-assembled plasmonic nanoparticle clusters. *Science* **2010,***328 (5982)*, 1135-1138.
(29) Hill, R. T.; Mock, J. J.; Hucknall, A.; Wolter, S. D.; Jokerst, N. M.; Smith, D. R.; Chilkoti, A. Plasmon ruler with angstrom length resolution. *Acs Nano* **2012,***6 (10)*, 9237-9246.
(30) Zhu, W.; Esteban, R.; Borisov, A. G.; Baumberg, J. J.; Nordlander, P.; Lezec, H. J.; Aizpurua, J.; Crozier, K. B. Quantum mechanical effects in plasmonic structures with subnanometre gaps. *Nat. Commun.***2016,***7*, 11495.
(31) Tame, M. S.; McEnery, K. R.; Oezdemir, S. K.; Lee, J.; Maier, S. A.; Kim, M. S. Quantum plasmonics. *Nat. Phys.***2013,***9 (6)*, 329-340.
(32) Scholl, J. A.; Garcia-Etxarri, A.; Koh, A. L.; Dionne, J. A. Observation of quantum tunneling between two plasmonic nanoparticles. *Nano Lett.***2013,***13 (2)*, 564-569.
(33) Savage, K. J.; Hawkeye, M. M.; Esteban, R.; Borisov, A. G.; Aizpurua, J.; Baumberg, J. J. Revealing the quantum regime in tunnelling plasmonics. *Nature* **2012,***491 (7425)*, 574-577.
(34) Gallinet, B.; Martin, O. J. F. Influence of electromagnetic interactions on the line shape of plasmonic Fano resonances. *ACS Nano* **2011,***5 (11)*, 8999-9008.
(35) Chang, W.-S.; Lassiter, J. B.; Swanglap, P.; Sobhani, H.; Khatua, S.; Nordlander, P.; Halas, N. J.; Link, S.A plasmonic Fano switch. *Nano Lett.***2012,***12 (9)*, 4977-4982.
(36) Teperik, T. V.; Nordlander, P.; Aizpurua, J.; Borisov, A. G. Robust subnanometric plasmon ruler by rescaling of the nonlocal optical response. *Phys. Rev. Lett.***2013,***110 (26)*, 263901.
(37) Sönnichsen, C.; Reinhard, B. M.; Liphardt, J.; Alivisatos, A. P. A molecular ruler based on plasmon coupling of single gold and silver nanoparticles. *Nat. Biotechnol.* **2005,***23 (6)*, 741-745.
(38) Hentschel, M.; Schaeferling, M.; Weiss, T.; Liu, N.; Giessen, H. Three-dimensional chiral plasmonic oligomers. *Nano Lett.***2012,***12 (5)*, 2542-2547.